Ab initio static dielectric matrices from the density-functional approach. II. Calculation of the screening response in diamond, Si, Ge, and LiCl

Mark S. Hybertsen and Steven G. Louie
Department of Physics, University of California, Berkeley, California 94720
(Received 22 September 1986; revised manuscript received 22 December 1986)

The density-functional approach with *ab initio* pseudopotentials has been used to calculate the static dielectric matrices for diamond, Si, Ge, and LiCl. The dielectric matrices for a regular sample of points in the Brillouin zone are used to calculate the screening response of the crystals to external perturbations. The perturbations considered are a constant external electric field and an added point charge at various locations in the unit cell. Through these examples, the local fields in the screening are illustrated and a qualitative picture of the role of exchange and correlation (included in the local-density approximation) is obtained. Local fields in semiconductors and insulators are found both to be quantitatively important and to alter the qualitative features of the screening response.

I. INTRODUCTION

In the preceding paper[1] (referred to as I), we have discussed the *ab initio* calculation of static dielectric matrices within the density-functional approach.[2] The only major approximation is the use of the local-density approximation (LDA).[3] The full dielectric matrices include the local fields in the screening. In I, the details of the calculation were given and the detailed results for the dielectric matrices themselves for the four materials diamond, Si, Ge, and LiCl were presented. The importance of local fields was demonstrated using the idea of the dielectric band structure[4] and through their effect on the macroscopic dielectric function. The role of exchange and correlation as included in the LDA was illustrated in the same way. A key feature of our approach in I is that it allows *ab initio* calculation of the dielectric matrices on a regular grid of $\mathbf{q}$ points through the Brillouin zone. This is essential for describing the response of the crystal to nonperiodic perturbations, e.g., a point charge.

In the present paper, we illustrate the local fields and the effect of exchange and correlation by showing the dielectric response of the materials studied to specific types of perturbation. Previous work based on empirical pseudopotential or tight-binding band structures has illustrated several of the trends in screening.[5–9] However, with the exception of Ref. 9, these results have been restricted to periodic perturbations ($\mathbf{q}=\mathbf{0}$) or to perturbations in the long-wavelength limit (e.g., phonons for $\mathbf{q}\rightarrow\mathbf{0}$).[10] Here, the *ab initio* dielectric matrices over the full Brillouin zone are exploited to consider a broader range of perturbations. In particular, the screening of a localized perturbation is illustrated. Consideration of the examples conveys some physical intuition regarding the local fields that is otherwise difficult to obtain from the elements of the dielectric matrices themselves. There are many important local perturbations. The case of a point charge (electron) is important for the problem of quasiparticle energies where local fields play an important role.[11,12] Response to a substitutional impurity, hydrogen, or a positron are other examples. Previous work on point-charge perturbations has illustrated some aspects of the response based on a local orbital approach for the dielectric matrix.[9]

In Sec. II the microscopic response to a constant external electric field is considered. This makes contact with previous work[7] and illustrates the important polarizable parts of the crystal. Trends as a function of metallicity (diamond to Ge) and ionicity (Si to LiCl) are illustrated. The contribution of exchange and correlation is also shown. The screening of an added point charge at different points in the unit cell is shown in Sec. III. This provides a dramatic illustration of local fields. For example, the induced charge due to an added point charge in the bond center of Ge is quite different from that induced by the point charge in the interstitial region. Comparison is made to previous work.[9] Brief concluding remarks are given in Sec. IV.

II. RESPONSE TO A CONSTANT EXTERNAL FIELD

Because of charge inhomogeneity, the microscopic response of a semiconductor or insulator to a macroscopic perturbation varies considerably over the unit cell. Essentially, the spatial variations in the polarization of the constituent units of the crystal (e.g., the bonds of a covalent material) become evident.

Consider a long-wavelength external (longitudinal) electric field:

$$\mathbf{E}_{\text{ext}}=\lim_{\mathbf{q}\rightarrow 0}\hat{\mathbf{q}}E_0 e^{i\mathbf{q}\cdot\mathbf{r}}\ . \tag{1}$$

Under the assumption of a longitudinal field, the corresponding perturbing potential can be derived. The resulting density response is obtained from the polarizability matrix discussed in I. In real space, one finds

$$\rho_{\text{ind}}(\mathbf{r})=iE_0\sum_{\mathbf{G}}\lim_{\mathbf{q}\rightarrow 0}\frac{1}{|\mathbf{q}|}\chi_{\mathbf{G},\mathbf{G}'=0}(\mathbf{q})e^{i\mathbf{G}\cdot\mathbf{r}}\ . \tag{2}$$

The result is well defined for a given direction of $\mathbf{q}$ since

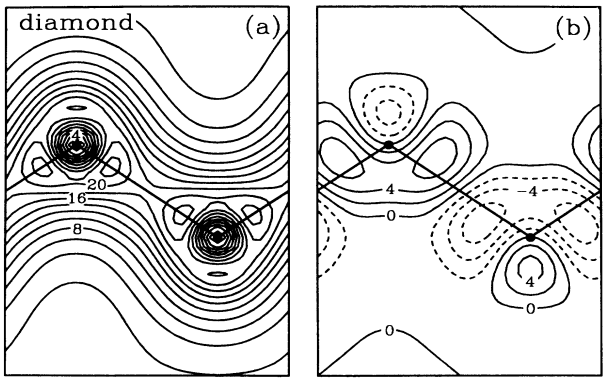

FIG. 1. In part (a) the pseudo valence charge from a self-consistent local-density functional calculation for diamond is plotted in the $1\bar{1}0$ plane. In part (b) the induced charge due to a constant applied electric field in the $\hat{\mathbf{z}}$ (vertical) direction of magnitude $eE_0=2$ Ry/a.u. The contour interval is 2 electrons per unit cell in both panels Negative contours are indicated by dashed lines. The bond chain is indicated schematically.

$\lim_{\mathbf{q}\to 0}\chi_{\mathbf{G},\mathbf{G}'=0}(\mathbf{q})$ is proportional to $|\mathbf{q}|$ for $\mathbf{G}\neq\mathbf{0}$. The microscopic response is thus strictly a local-field effect because $\chi_{00}(\mathbf{q})$ goes as q^2 for small $|\mathbf{q}|$.

The linear response to a uniform applied field has been calculated for the four materials diamond, Si, Ge, and LiCl. The vector $\mathbf{q}$ was taken to approach zero along the $\hat{\mathbf{z}}$ direction. The polarizability matrices described in I were used. These include of order 140 to 220 $\mathbf{G}$ vectors depending on material. Exchange-correlation effects are explicitly included using the local-density approximation. The results for the induced charge are given as a contour plot in the $(1\bar{1}0)$ plane of diamond, Si, and Ge in part (b) of Figs. 1—3. The induced charge for LiCl is displayed in a (010) plane in Fig. 4(b). (Note that the change in the number density of electrons is displayed.) Part (a) of each figure shows the valence charge density for the crystal as calculated from an *ab initio* pseudopotential calculation. This is provided for reference and ease of comparison. The units used in the plots are electrons per cell. This choice allows meaningful comparison among the four materials of generally different average electron density. All have eight electrons per unit cell. The corresponding cell volumes are given in a.u.^{3} along with other useful data for each material in Table I.

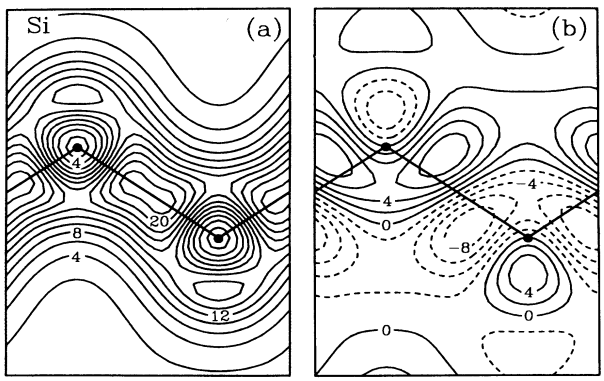

FIG. 2. Same as Fig. 1 for Si.

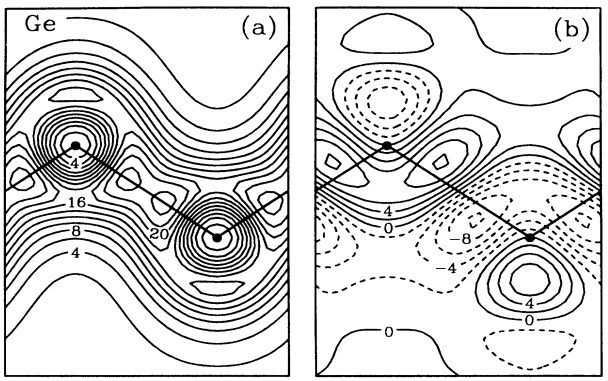

FIG. 3. Same as Fig. 1 for Ge.

We start by considering the series of homopolar materials. The polarizable unit in this case is the bond. There is a chain of bonds in the plane of the figure (indicated schematically in Figs. 1—3). The maxima in the charge density associated with the bond are evident, with the case of diamond exhibiting a strong two-peak structure.[13] There is also another pair of bonds associated with each atom in the figure in a plane perpendicular to the page. This gives rise to the smaller relative maxima seen in the plane of the figures. The charge density at the atomic sites is low since only the valence electrons in the pseudopotential formalism are considered. In units of electrons per cell, the maxima in the charge density are about the same in all three materials.

Application of the external field causes electrons to be pushed across the bonds. All the bonds in the crystal are at an angle to the direction of the applied field considered here. A dipole is established on each bond. However, the dipole does not appear to be parallel to the applied field. This is a consequence of the directionality of the bonds. The covalent bonds are not spherically symmetric objects and the induced charge reflects the shape of the bonds to some degree. The polarizability along the bond is larger than in the transverse direction. Although the microscopic dipoles associated with each bond are not aligned with the external field, the net macroscopic polarization field is parallel to $\mathbf{E}_0$. Quantitatively, the induced charge is

TABLE I. The cell volume, corresponding r_s, and Thomas-Fermi wave vector q_{TF} are tabulated for the four materials studied here.

	Ω_c (a.u.^{3})	r_s (a.u.)	q_{TF} (a.u.$^{-1}$)
Diamond	76.61	1.317	1.36
Si	270.01	2.005	1.10
Ge	304.89	2.088	1.08
LiCl	228.17	1.895	1.14

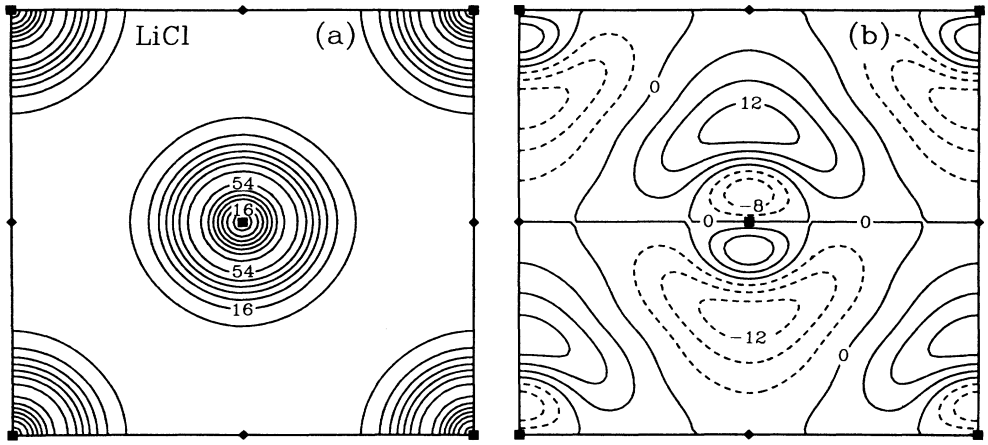

FIG. 4. In part (a) the pseudo valence charge for LiCl is plotted in the (010) plane. The contour interval is 8 electrons per unit cell. In part (b) the induced charge due to a constant applied electric field in the $\hat{z}$ (vertical) direction of magnitude $eE_0=2$ Ry/a.u. The contour interval is 4 electrons per unit cell. The atomic sites are indicated, Li by a solid diamond and Cl by a solid square.

smallest for diamond and largest for Ge when taken relative to the average density (or peak density). This is intuitively reasonable in so far as it follows the trend in the dielectric constants for the materials. The material of larger metallicity (Ge) is more polarizable.

The results described here are consistent with the work of Baldereschi and Resta[6,7] based on empirical pseudopotential band structures. Their results for the induced charge due to an external field parallel to the bond in the (111) direction show polarization of about the same magnitude.

The response of the ionic crystal LiCl is shown in Fig. 4. The Cl ions are the polarizable units in this case. There is very little charge remaining on the Li sites as shown in Fig. 4(a). The Cl sites are also relative minima in the charge density with the largest density being at the peak of the $3p$ wave function for the Cl ions. The induced charge shown in Fig. 4(b) reflects these observations. The primary effect is polarization of the Cl ions. The electrons are pushed from one side of the Cl ion to the other. In addition, electrons are pushed across the peak in the valence charge density. This accounts for the node in ρ_{ind} located near the peak of the $3p$ wave functions. Quantitatively, the proportion of the valence charge displaced per unit electric field strength is smaller than in the homopolar cases. This is consistent with the smaller dielectric constant in LiCl.

The induced charge shown in Figs. 1—4 all included the effect of exchange and correlation. It is straightforward to illustrate the role of exchange and correlation by dropping K_{xc} from the calculation of χ leaving the usual random-phase approximation (RPA) response function. [See Eq. (10) in I.] In Fig. 5, the *difference* between the induced charge with and without exchange-correlation effects is shown for the three homopolar materials. The same is shown for LiCl in Fig. 6. What is apparent is that the inclusion of exchange-correlation effects in the screening explicitly gives 10—20% *more effective* screening.

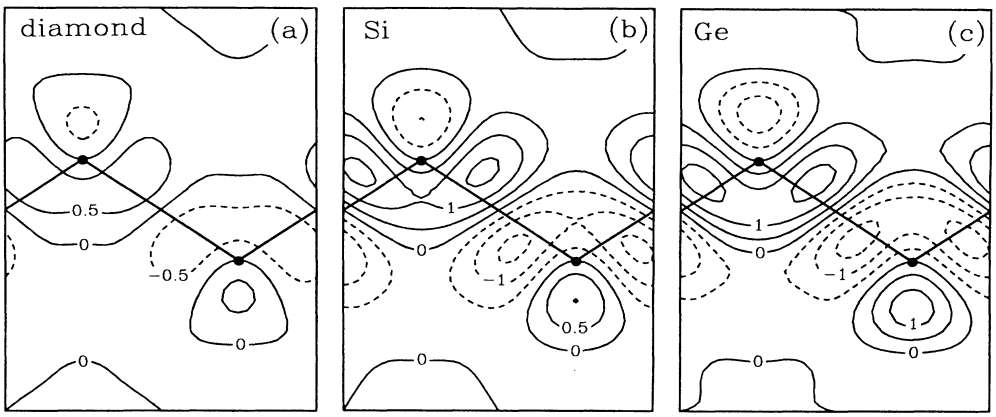

FIG. 5. The portion of the induced charge due to the exchange-correlation effects in the polarizability from a constant applied external electric field as in Figs. 1—3. The cases of diamond (a), Si (b), and Ge (c) are shown. The contour interval is 0.5 electrons per unit cell.

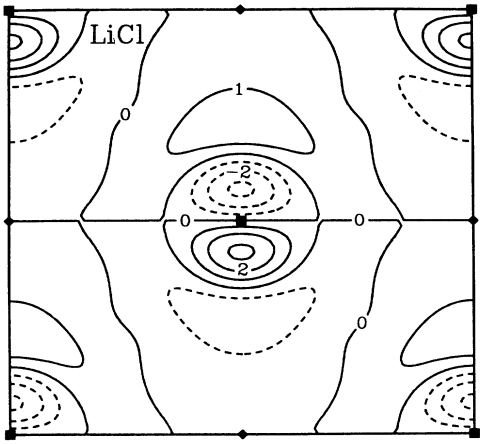

FIG. 6. The portion of the induced charge due to the exchange-correlation effects in the polarizability from a constant applied external electric field as in Fig. 4 for LiCl. The contour interval is 1.0 electrons per unit cell.

This arises physically because the exchange-correlation energy is negative and thus favors building up of charge (e.g., bonding). In the case of the screening response, a deeper corrugation in the density is possible to lower the total energy of the perturbed system. The trends described in I for the relative importance of exchange-correlation effects are also seen here. The effect is larger in Ge and Si as compared to diamond and LiCl. This is consistent with the larger average value of r_s in Si and Ge.

III. RESPONSE TO A POINT-CHARGE PERTURBATION

In the example of the added point charge, the induced potential is a full two-point function, $V_{\rm scr}(\mathbf{r},\mathbf{r}')$. This is due to the local fields; the screening potential depends on $\mathbf{r}-\mathbf{r}'$ if only the diagonal part of the dielectric matrix is included. The details of the full screening potential depend dramatically on the location of the added charge $\mathbf{r}'$ and in general the screening potential is anisotropic. These aspects of local fields are illustrated in this section.

The expression for the electrostatic screening potential seen by a test probe Ze around an added point charge $Z'e$ is straightforward to derive in terms of the dielectric matrix:

$$V_{\rm scr}(\mathbf{r},\mathbf{r}')=\sum_{\mathbf{q},\mathbf{G},\mathbf{G}'} e^{i(\mathbf{q}+\mathbf{G})\cdot\mathbf{r}}[\epsilon^{-1}_{\mathbf{G}\mathbf{G}'}(\mathbf{q},\omega=0)-\delta_{\mathbf{G}\mathbf{G}'}] \times\frac{4\pi ZZ'e^2}{\Omega\,|\,\mathbf{q}+\mathbf{G}'\,|^2}e^{-i(\mathbf{q}+\mathbf{G}')\cdot\mathbf{r}'}\,. \tag{3}$$

The usual Coulomb interaction is present as the perturbation from the point charge of magnitude $Z'e$ at $\mathbf{r}'$. In the case where the dielectric matrix is zero for $\mathbf{G}\neq\mathbf{G}'$ (local fields are negligible), this expression reduces to being a function of $\mathbf{r}-\mathbf{r}'$ as noted above. Derivation of $\rho_{\rm scr}(\mathbf{r},\mathbf{r}')$ follows directly from Poisson's equation and brings in an extra factor of $|\,\mathbf{q}+\mathbf{G}\,|^2$ in Eq. (3). The case considered here is $Z=Z'=-1$ (relevant for the quasiparticle problem[11,12]).

In evaluating Eq. (3), eight $\mathbf{q}$ points were used in the irreducible wedge of the Brillouin zone. (One should note that these must be unfolded to the full Brillouin zone in practice to obtain the screening potential at general points $\mathbf{r}$.) The details of the technique used for the Brillouin-zone summation and handling the Coulomb interaction are given elsewhere.[11] The full dielectric matrices available from I were used including exchange-correlation effects appropriate for a test-charge probe of the screening potential. These include approximately 140 to 220 $\mathbf{G}$ vectors depending on material and $\mathbf{q}$. The results presented here are converged to 10% or better with respect to the size of the dielectric matrix and the Brillouin-zone summation. One should note that the extra factor of $|\,\mathbf{q}+\mathbf{G}\,|^2$ required for $\rho_{\rm scr}$ leads to more difficulties with convergence. The results presented for $\rho_{\rm scr}$ are reliable out to a radius of about 6 a.u. around $\mathbf{r}'$.

The local-field contribution can be simply illustrated by considering the screening potential at the site of the perturbing charge, $V_{\rm scr}(\mathbf{r},\mathbf{r})$. The response is sensitive to the charge inhomogeneity with the bond chain being more polarizable than the interstitial region. Thus, the $V_{\rm scr}(\mathbf{r},\mathbf{r})$ depends on $\mathbf{r}$. This is strictly due to the local fields; neglecting the off-diagonal elements of the dielectric matrix leads to $V_{\rm scr}(0)$ independent of $\mathbf{r}$. The role of local fields for the four materials studied here is summarized in Table II. The first row gives $V_{\rm scr}(\mathbf{r},\mathbf{r})$ without local fields. This is obtained by including only the $\mathbf{G}=\mathbf{G}'$

TABLE II. The screening potential acting upon a test probe ($Z=-1$) at $\mathbf{r}$ due to a negative unit charge ($Z'=-1$) at $\mathbf{r}$ [i.e., $V_{\rm scr}(\mathbf{r},\mathbf{r})$] is shown for the materials studied here and for $\mathbf{r}$ at several symmetry sites. For comparison, the screening potential without local fields is also shown. The latter is independent of $\mathbf{r}$. The potentials are given in Ry.

Site	Diamond	Si	Ge	LiCl
No local fields	−1.72	−1.40	−1.34	−0.97
With local fields				
Atomic	−2.46	−1.37	−1.25	−0.65(Li) −1.92(Cl)
Bonding	−2.05	−1.84	−1.74	
Antibonding	−1.77	−1.48	−1.42	
Hexagonal	−1.09	−0.87	−0.82	

terms of the summation in Eq. (3). The succeeding rows give the full case including local fields for different sites in the unit cell: on the atoms, in the center of the bond, in the corresponding antibonding site [i.e., along the (111) direction past the atom towards the interstitial region], and in the interstitial region (hexagonal site).

Consider first the case of LiCl. For the case of the added charge on the Cl site, the local fields enhance the screening potential. This is intuitively reasonable since most of the valence charge density is accumulated around the Cl ions. In contrast, for the case of the added charge on the Li site, the local fields reduce the screening potential. There is very little charge near the Li sites leading to significantly less screening. For the homopolar materials Si and Ge, the bond is the most polarizable unit. Local fields lead to enhanced screening of a point-charge perturbation in the center of the bond. On the other hand, the screening potential is significantly reduced by the local fields for the case of a perturbation in the interstitial region. For the atomic sites, the net effect of local fields is small. Although the charge on the atomic sites is quite small (see Figs. 2 and 3), the tetrahedral bonds are symmetrically placed about each atom. The perturbing charge polarizes these bonds leading to a substantial screening potential. In diamond, the peak charge density in the bonds is sufficiently close to the atomic sites that the resulting screening potential is larger for the on-site case than for the bond-center case. This is probably related to the pronounced double peak structure specific to the carbon bond. Otherwise, the local-field effects in diamond are similar to Si and Ge.

The trend in the magnitudes can be understood in terms of the changes in density as well as metallicity (gap size). Using a Thomas-Fermi model for the dielectric function results in

$$V_{\rm scr}(0) = -ZZ'e^2 q_{\rm TF} \ . \tag{4}$$

This then suggests that materials with lower density will have a smaller screening potential. Referring to the values of $q_{\rm TF}$ for the average density given in Table I, diamond should have a larger screening response than Si, which is, in turn, larger than Ge. This is consistent with the results in Table II without local fields. (The Thomas-Fermi model does not take local fields into account.) However, on this basis, LiCl should exhibit a larger screening potential than Si and Ge, contrary to Table II. Furthermore, Eq. (4) is in poor quantitative agreement with our accurate results. There are two reaons for this. First, the Thomas-Fermi model dielectric function is only valid for small $\mathbf{q}$, whereas $V_{\rm scr}(\mathbf{r}=0)$ depends on the large $\mathbf{q}$ behavior of ϵ. Second, the small-$\mathbf{q}$ screening in the insulators is significantly different than in the metallic Thomas-Fermi model. In particular, for materials with a small dielectric constant such as LiCl, the point perturbation is significantly less screened. This accounts for the less effective screening (without local fields) in LiCl as compared to Si and Ge. The competing effects of the density and the metallicity determine the magnitude of the screening response.

Having discussed these basic trends in the screening response and the role of local fields, we turn to specific examples to provide a more detailed picture. The induced charge exhibits many more details of the response to the added point charge than the screening potential. The latter averages over the induced charge:

$$V_{\rm scr}(\mathbf{r},\mathbf{r}') = -\int d\mathbf{r}'' \frac{Ze^2}{|\mathbf{r}-\mathbf{r}''|} \rho_{\rm scr}(\mathbf{r}'',\mathbf{r}') \ . \tag{5}$$

(The $\rho_{\rm scr}$ is taken as a number density with the charge indicated explicitly.) Also, due to the incomplete screening in semiconductors and insulators, $V_{\rm scr}$ is long range. Results are given here for Ge representative of the homopolar materials and for LiCl.

In Fig. 7, the induced charge around a negative point charge ($Z'=-1$) in the bond center is depicted for the case of Ge. Figure 7(a) shows the induced charge without local fields ($\mathbf{G}=\mathbf{G}'$ terms only). It is spherically symmetric and centered on the added charge.[14] Negative con-

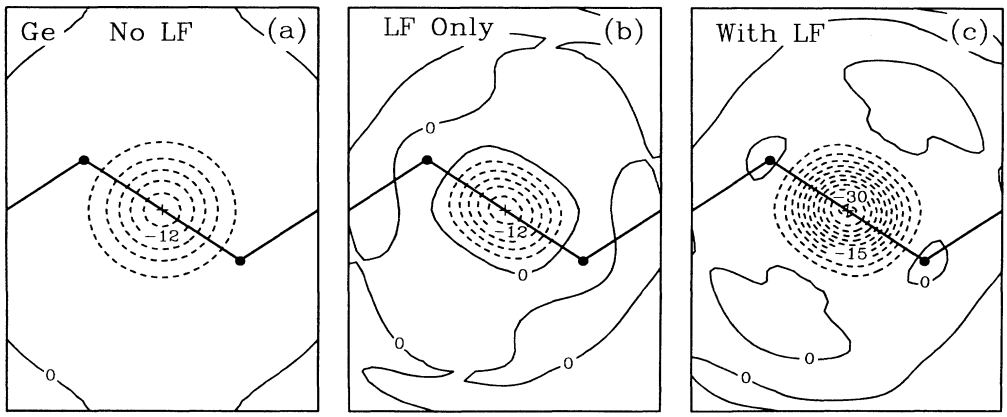

FIG. 7. The induced change in electron number density due to a negative point-charge perturbation of magnitude e at the center of the bond is shown for the case of Ge. In part (a) only the diagonal part of the dielectric matrix is included (no local fields). In part (b) only the off-diagonal part is included (local fields only). In part (c) the total induced change is plotted. The contour interval is 3 electrons per unit cell. The site of the added point charge is indicated by a cross (+).

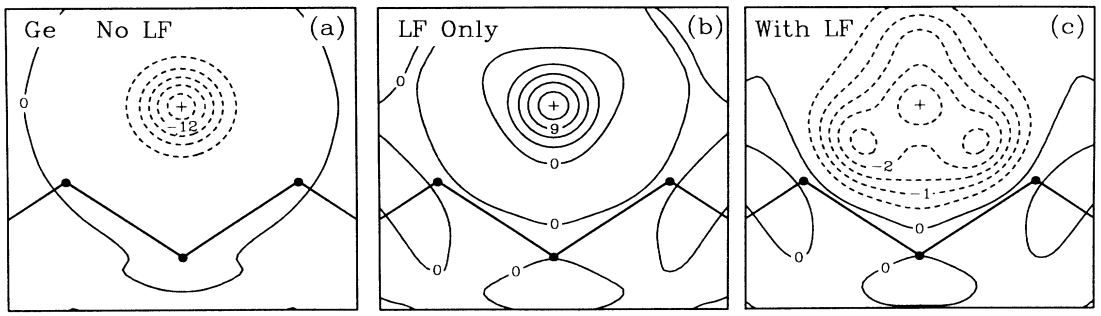

FIG. 8. Same as Fig. 7 but for a negative point charge in the interstitial region (hexagonal site). The contour interval is 3 electrons per cell in (a) and (b). The contour interval is 0.5 electrons per cell in (c).

tours are dashed and the density is reduced near the perturbation. The contribution of the local fields is isolated in Fig. 7(b) ($\mathbf{G}\neq\mathbf{G}'$ terms only). Several features are evident. First, the response is deepened in the bond. The bond region is more polarizable than the average density. This is quantitatively quite important. Near the perturbation, the local-field contribution is just as large as the average response given in Fig. 7(a). Second, some of the charge pushed out of the bond accumulates around the outside of the bond and on the atomic sites (region of positive induced density). Thirdly, there is polarization of the neighboring bonds. This is evident from the nodal surfaces that bisect the other two bonds in the plane of the page. Only half of each of these bonds is shown terminated by the edge of the figure. Charge is pushed out of the part of those bonds seen in the figure into the other half of the bond. There is similar polarization of the bonds in the plane perpendicular to the figure, although this is less evident from the figure. In Fig. 7(c), the net induced charge is plotted including both the diagonal contribution as well as the local fields. The local fields contribute about half the response near the perturbation. In addition, the polarization of the six neighboring bonds is still evident as well as the charge pushed out into the interstitial region.

Figure 8 depicts the same contributions to the induced charge, but for the case of a perturbation in the interstitial region (hexagonal site). The diagonal part in Fig. 8(a) is the same as that shown in Fig. 7(a) but now centered around the hexagonal site. The local-field contribution in Fig. 8(b) is now positive, indicating that the local fields reduce the response substantially. Also, tracking the nodal surfaces in Fig. 8(b) reveals the polarization of all the surrounding bonds. Some electrons are moved across the bonds below the hexagonal site; the part of the bond near the perturbation is depleted while the other side of the bond is enhanced somewhat. The bonds along (111) and $(11\bar{1})$ are polarized in the longitudinal direction. The bonds in the plane perpendicular to the figure are similarly polarized. The net induced charge depicted in Fig. 8(c) dramatically illustrates the nonsphericity of the response of the full crystal including local fields. There are maxima in the induced charge displaced from the site of the perturbation toward the regions of higher charge density in the bonds. The polarization of the neighboring bonds is still evident. Finally, the depth of the induced charge is considerably smaller with the inclusion of local fields. It is consequently more spread out. Note that integrated over the crystal, $1-1/\epsilon_0$ electrons are displaced independent of the detailed arrangement or inclusion of local

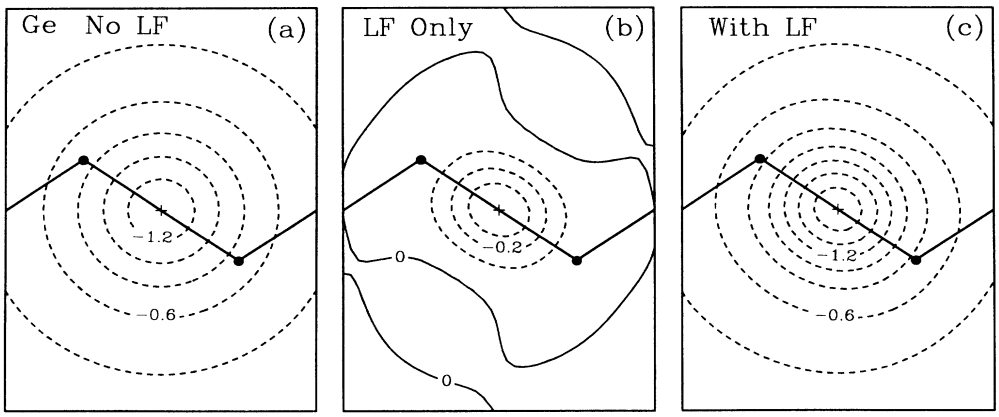

FIG. 9. The screening potential seen by a test probe ($Z=-1$) due to a negative point-charge perturbation at the center of the bond is plotted for the case of Ge. The figure is arranged as in Fig. 7. The contour interval is 0.2 Ry in (a) and (c) but is 0.1 Ry in (b).

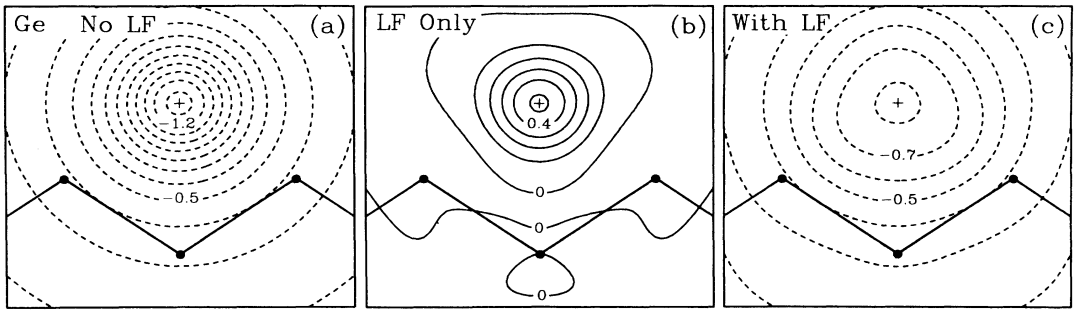

FIG. 10. Same as Fig. 9 but for a negative point charge in the interstitial region (hexagonal site). The contour interval is 0.1 Ry.

fields. This follows from the $\mathbf{q}\rightarrow 0$ limit of $\epsilon^{-1}(\mathbf{q})$ and proper definition of the macroscopic dielectric constant ϵ_0 as described in I.

Next we consider the corresponding screening potential. Figure 9 depicts the screening potential seen by a test particle ($Z=-1$) due to an added charge ($Z'=-1$) at the bond center in Ge. The response to a point charge in the interstitial is shown in Fig. 10. The three panels of the figures are the same as for the induced charge shown in Figs. 7 and 8. Neglecting local fields results in a spherically symmetric screening potential independent of $\mathbf{r}'$. The local-field contribution in Figs. 9(b) and 10(b) primarily alters the response near the perturbation. In the bond-center case, the screening potential is enhanced, whereas in the interstitial case, it is reduced. (This trend was also observed in Table II.) In addition, the local-field contribution introduces asymmetries in the response. These reflect, in a convoluted way, the microscopic polarization of the bonds. Comparison to Figs. 7 and 8 shows that much of the detail is washed out but that the overall features remain. The response to the bond-center perturbation is elongated along the direction of the bond and somewhat reduced in the interstitial region. In the interstitial case, the response is extended towards the bonds and retains the triangular symmetry seen in Fig. 8(c). The detailed polarization of the neighboring bonds described above has a small impact on the shape of the net screening potential. Although evident in the local-field contribution in part (b) of each figure, these small oscillations are not apparent in part (c). The long-range tail of the screening potential is much larger. Finally, unlike a metal, the screening potential is long range, as is readily evident in the figures. Given the values of q_{TF} in Table I, metallic screening would give the response a range of only 1—2 a.u.

A similar study showing the response to a positive point-charge perturbation in diamond and Si has been performed by Mattausch *et al.*[9] The results are in qualitative agreement with those found in the present work. In particular, the structure of the response to an interstitial perturbation in Si conforms closely to the results shown here in Figs. 8(c) and 10(c) for Ge. Mattausch *et al.* included exchange effects using the time-dependent screened Hartree-Fock approximation (the ladder bubble diagrams). The net effect is similar to that found here using the LDA and illustrated in Sec. II: The screening is more effective.

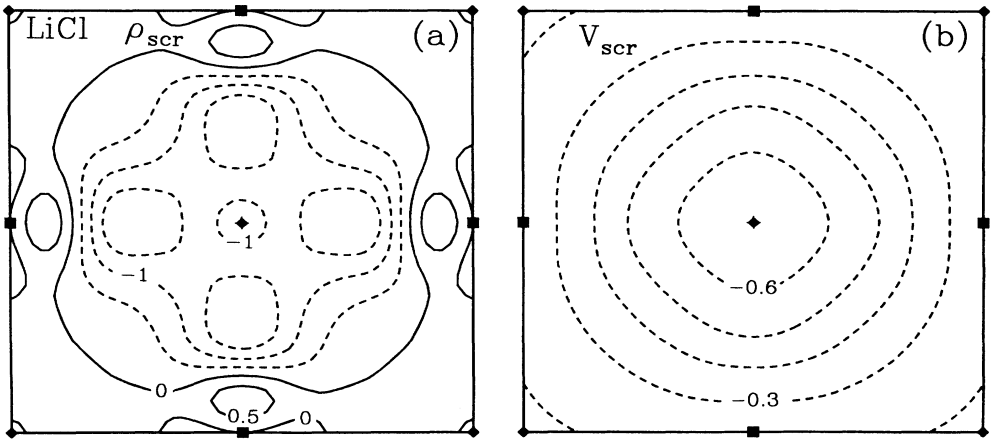

FIG. 11. The induced change in electron number density (a) and screening potential seen by a test probe (b) due to a negative point-charge perturbation of magnitude e on the Li site (indicated by solid diamond) in LiCl is plotted. The contour interval in (a) is 0.5 electrons per unit cell and in (b) is 0.1 Ry.

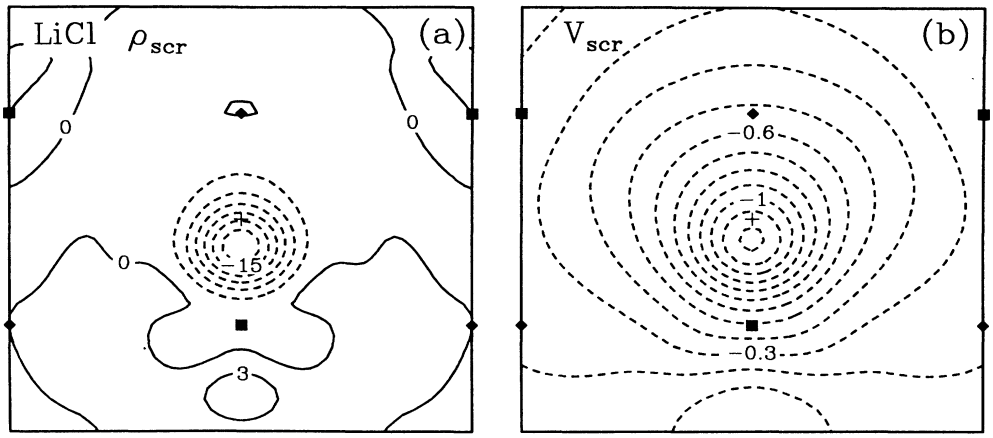

FIG. 12. Same as Fig. 11 but for a negative point charge halfway between the Li and Cl sites (indicated by +) in LiCl. The contour interval in (a) is 3 electrons per unit cell and in (b) is 0.1 Ry.

The quantitative role of exchange-correlation reported in Ref. 9 is consistent with the LDA results here for the static response (included but not separated out explicitly). However, the quantitative importance of local fields is significantly greater in the present study than shown in Ref. 9 for the interstitial perturbation. One might expect the tight-binding basis to be less adequate for that case.

The local fields fulfill a similar role in the ionic compound LiCl. The response to an added negative point charge on the Li site is plotted in Fig. 11. The net induced charge (a) and screening potential (b) are shown. The case of a perturbation halfway between a Li and a Cl site in the (010) plane is given in Fig. 12. Recalling from Sec. II that the Cl ions are the dominant polarizable unit, the structure of the induced charge in each case is clear. There is very little charge on the Li site, but the added charge polarizes the neighboring Cl ions. The maxima in Fig. 11(a) are all displaced toward the Cl ions. The nodal surface passes through the region near the peaks in the Cl $3p$ wave functions. Charge is transferred from the outer region of the Cl ions (near the perturbation on the Li site) to the region nearer the Cl sites. In addition, some charge is pushed across the whole Cl ions, although this is out of the figure. The corresponding screening potential [Fig. 11(b)] is significantly reduced by the local fields and has taken on the fourfold symmetry of the Li site in this plane.

For the case of the perturbation between the Li and Cl sites, the position of the added point charge $\mathbf{r}'$ is outside the peak in the Cl $3p$ wave functions. The resulting induced charge has its peak displaced from the site of the perturbation into the region of higher density. This is purely a local-field effect. Also, some of the charge is displaced in the regions around the Li sites and a small polarization of the other two Cl ions in the figure is evident. The corresponding screening potential is highly asymmetric. The peak is displaced from $\mathbf{r}'$. The nearest-neighbor Cl ion concentrates the screening response near the perturbation. However, beyond this Cl ion, the response is reduced. That region appears to be shielded to some degree by the Cl ion.

As a final note, the results given here all include the effect of exchange and correlation within the LDA. Comparison to RPA results shows the same trend as that illustrated in Sec. II for the uniform perturbation. Namely, the response of the crystal is enhanced in each case by inclusion of exchange-correlation effects. This applies both to the diagonal part of the response as well as to the local-field contribution with the effect being roughly proportional. The tight-binding-based results of Mattausch *et al.*[9] show a similar trend for exchange effects with some differences in detail.

IV. CONCLUDING REMARKS

The local fields in the microscopic dielectric response of semiconductors and insulators are shown to be quantitatively quite important. The resulting induced charge from a uniform or point-charge perturbation varies considerably from that given by the average density. The local fields describe the variation in the polarization of different parts of the unit cell. As extensively shown here, the polarization of the bonds in the homopolar materials depends on the source and nature of the perturbation. For the ionic material LiCl, the predominance of the Cl ion as the polarizable unit in the crystal is reproduced by the local fields. Although the chemical origin of these variations is quite different in the homopolar and ionic cases, the dielectric matrix includes the microscopic variation in the polarizability in both cases. The dielectric matrix approach thus unifies the description of the screening response in a single formulation.

ACKNOWLEDGMENTS

This work was supported by National Science Foundation Grant No. DMR-83-19024. The work was facilitated by the IBM Distributed Academic Computing Environment at the University of California, Berkeley. One of us (S.G.L.) wishes to acknowledge support by the Miller Institute.

[1]M. S. Hybertsen and S. G. Louie, preceding paper, Phys. Rev. B **35**, 5585 (1987).
[2]P. Hohenberg and W. Kohn, Phys. Rev. **136**, B864 (1964).
[3]W. Kohn and L. J. Sham, Phys. Rev. **140**, A1133 (1965).
[4]A. Baldereschi and E. Tosatti, Solid State Commun. **29**, 131 (1979).
[5]A. Baldereschi and E. Tosatti, Phys. Rev. B **17**, 4710 (1978).
[6]R. Resta and A. Baldereschi, Phys. Rev. B **23**, 6615 (1981).
[7]A. Baldereschi and R. Resta, in *Ab Initio Calculation of Phonon Spectra,* edited by J. T. Devreese, V. E. Van Doren, and P. E. Van Camp (Plenum, New York, 1983), p. 1.
[8]A. Fleszar, Ph.D. thesis, ISSA, University of Trieste, 1985 (unpublished).
[9]H. J. Mattausch, W. Hanke, and G. Strinati, Phys. Rev. B **27**, 3735 (1983).
[10]Several illustrations of local fields given in Ref. 8 overlap somewhat with the present discussion but with emphasis on the phonon problem.
[11]M. S. Hybertsen and S. G. Louie, Phys. Rev. Lett. **55**, 1418 (1985); Phys. Rev. B **32**, 7005 (1985); **34**, 5390 (1986).
[12]G. Strinati, H. J. Mattausch, and W. Hanke, Phys. Rev. Lett. **45**, 290 (1980); Phys. Rev. B **25**, 2867 (1982).
[13]This is discussed in M. T. Yin and M. L. Cohen, Phys. Rev. B **24**, 6121 (1981).
[14]For the crystalline case, neglect of local fields does not strictly guarantee spherical symmetry. The dielectric response is not isotropic in **q**. These effects, however, are difficult to distinguish from variations arising from the finite sampling of the Brillouin zone and truncation of the **G**-space summations.